HHS Public Access

Author manuscript

Sci Signal. Author manuscript; available in PMC 2017 August 21.

Published in final edited form as:

Sci Signal. ; 9(458): ra123. doi:10.1126/scisignal.aai7884.

Essential roles of AMPA receptor GluA1 phosphorylation and presynaptic HCN channels in fast-acting antidepressant responses of ketamine

Ke Zhang[1], **Ting Xu**[1,2,*], **Zhongmin Yuan**[1,*], **Zhisheng Wei**[2,*], **Vitor Nagai Yamaki**[1], **Mingfa Huang**[2], **Richard L. Huganir**[3], and **Xiang Cai**[1,†]

[1]Department of Physiology, Southern Illinois University School of Medicine, 1135 Lincoln Drive, Carbondale, IL 62901, USA

[2]The Institute of Neuroscience, the Second Affiliated Hospital of Guangzhou Medical University, 250 Changgang Road, Guangzhou, Guangdong 51030, China

[3]The Solomon H. Snyder Department of Neuroscience, Howard Hughes Medical Institute, Johns Hopkins University School of Medicine, 725 North Wolfe Street, Baltimore, MD 21205, USA

Abstract

Although the molecular mechanism is not clear, the clinically tested drug ketamine has rapid antidepressant action that does not require the multiple weeks of treatment needed for other antidepressant drugs to have an effect. We showed that ketamine potentiated Schaffer collateral–CA1 cell excitatory synaptic transmission in hippocampal slice preparations from rodents and enhanced the phosphorylation of the GluA1 subunit on Ser^{845} of the AMPA-type glutamate receptor in the hippocampal area CA1. These effects persisted when γ-aminobutyric acid (GABA) receptors were pharmacologically blocked. Ketamine reduced behavioral despair in wild-type mice but had no effect in GluA1 S845A knock-in mutant mice. Presynaptic (CA3 pyramidal cell), but not postsynaptic (CA1 pyramidal cell), deletion of N-methyl-D-aspartate (NMDA)–type glutamate receptors eliminated the ketamine-induced enhancement of excitatory synaptic transmission in hippocampal slices and the antidepressant actions of ketamine in mice. The synaptic and behavioral actions of ketamine were completely occluded by inhibition or deletion of the hyperpolarization-activated cyclic nucleotide–gated channel 1 (HCN1). Our results implicate presynaptic NMDA receptor inhibition followed by reduced activity of presynaptic HCN1 channels, which would result in an increase in glutamate release and postsynaptic glutamate

†Corresponding author. cai001@siu.edu.
*These authors contributed equally to this work.

SUPPLEMENTARY MATERIALS

www.sciencesignaling.org/cgi/content/full/9/458/ra123/DC1

Author contributions: K.Z., T.X., V.N.Y., and X.C. performed and analyzed the electrophysiological as well as behavioral experiments. K.Z., Z.Y., Z.W., and M.H. performed membrane protein biotinylation and Western blot experiments. R.L.H. offered GluA1 S845A mice and provided suggestions on manuscript submission. X.C. designed the study and prepared the manuscript and figures.

Competing interests: The authors declare that they have no competing financial interests.

Data and materials availability: All data and materials are commercially available.

receptor activity, as a mechanism of ketamine action. These data provide a mechanism for changes in synaptic activity that could explain the fast-acting antidepressant effects of this drug.

INTRODUCTION

Major depressive disorder (MDD) is a serious public health problem with a lifetime prevalence of 7 to 12% in men and 20 to 25% in women (1–3). Existing treatments for MDD usually take weeks to months to achieve their antidepressant effects, and many patients do not experience adequate improvement even after months of treatment (4). Clinical trial data showed that a single subanesthetic dose (0.5 to 10 mg/kg) of ketamine, a noncompetitive ionotropic glutamatergic *N*-methyl-D-aspartate (NMDA) receptor antagonist, produced rapid and sustained antidepressant responses in patients suffering from MDD (4–6). However, the psychotomimetic (psychosis-producing) properties and abuse potential of ketamine necessitate caution in promoting this compound as a general treatment for depression (7). Understanding the underlying mechanism responsible for ketamine's beneficial behavioral effects may be the key to developing novel, safe, and fast-acting antidepressants.

Most studies indicate that the antidepressant action of ketamine requires synaptic protein synthesis and AMPA-type glutamate receptor activation (8–10). However, the upstream mechanism responsible for ketamine-induced AMPA receptor potentiation is controversial, as is the mechanism underlying how ketamine promotes the increase in synaptic protein synthesis.

Here, we report a presynaptic effect of ketamine that is required for its rapid antidepressant actions. We examined the effect of ketamine on excitatory synaptic transmission in the hippocampus, a key brain region involved in memory consolidation and antidepressant actions (11–13). Because the GluA1 subunit of the AMPA receptor is phosphorylated at Ser^{845} and this phosphorylation promotes the insertion of GluA1 subunit–containing AMPA receptors into synaptic membrane (14), we examined the requirement of phosphorylation at this site for the behavioral and electrophysiological effects of ketamine and examined the signaling pathways involved. We explored the role of pre- and postsynaptic NMDA–type glutamate receptors in mediating ketamine's antidepressant and electrophysiological effects. Mice lacking hyperpolarization-activated cyclic nucleotide–gated channel 1 (HCN1), which is important for synaptic plasticity and dendritic integration (15), do not respond to the antidepressant effects of ketamine (16); therefore, we investigated the role of HCN1 in mediating the effects of ketamine. Our results identified a presynaptic mechanism, involving NMDA receptor (NMDAR) and HCN1 inhibition, which resulted in enhanced AMPA receptor phosphorylation and surface abundance, as important for the antidepressant effects of ketamine.

RESULTS

Ketamine enhances synaptic transmission and GluA1 phosphorylation through a protein kinase A–dependent pathway

To elucidate the mechanism that underlies the fast and long-lasting antidepressant action of ketamine, we examined the impact of ketamine on excitatory synaptic transmission in the hippocampus. Field excitatory postsynaptic potentials (fEPSPs) in stratum radiatum were recorded by stimulating Schaffer collateral pathways (SC-CA1 fEPSPs) at a frequency of 0.05 Hz in hippocampal slices prepared acutely from young adult Sprague-Dawley rats. Bath application of (*R*,*S*)-ketamine increased the slope of these fEPSPs (Fig. 1A). Ketamine was potent, with a significant effect seen at a concentration of 10 nM and an EC_{50} (median effective concentration) of 53 nM (Fig. 1B).

Phosphorylation of the AMPA receptor on GluA1 subunits enhances AMPA receptor–mediated synaptic currents. Ser^{845} of GluA1 is present in a consensus phosphorylation site motif for protein kinase A (PKA) (17). Pretreatment of hippocampal slices with H89, a PKA inhibitor, completely blocked ketamine-induced potentiation of SC-CA1 fEPSPs (Fig. 1A). Using CA1 tissue wedges dissected from the hippocampal slices, we analyzed the abundance ofGluA1 and phosphorylation of Ser^{845} by Western blotting. Bath application of ketamine significantly increased the phosphorylation of GluA1 Ser^{845} and the abundance of total GluA1, with effects observed as soon as 15 min after ketamine exposure (Fig. 1C).H89 pretreatment blocked the ketamine-induced increase in GluA1 Ser^{845} phosphorylation, but not the increase in total GluA1 abundance (Fig. 1D). Complementing this observation, pretreatment of hippocampal slices with anisomycin, a protein synthesis inhibitor, had no effect on either ketamine-induced potentiation of SC-CA1 fEPSPs or GluA1 Ser^{845} phosphorylation but blocked the ketamine-induced increase in GluA1 abundance (Fig. 1, E and F). In addition, K252a (a Trk receptor inhibitor), but not H89 or KN62 [calcium/calmodulin-dependent protein kinase II (CaMKII) inhibitor], completely blocked ketamine-induced enhancement of GluA1 abundance (Fig. 1G). These results indicated that ketamine enhanced the phosphorylation and increased the abundance of GluA1 through distinct mechanisms.

Ketamine increases the abundance of GluA1 at the cell surface and induces rapid antidepressant-like responses in the forced swim test

GluA1 Ser^{845} phosphorylation promotes the rapid insertion of GluA1 subunit–containing AMPA receptors into the postsynaptic membrane (14). To test the effect of ketamine on membrane surface abundance of AMPA receptors at SC-CA1 synapses, we performed membrane surface protein biotinylation experiments. Ketamine increased the abundance of GluA1 at the membrane surface. H89 pretreatment blocked this increase in GluA1 at the cell surface without affecting the ketamine-induced increase in total GluA1 abundance (Fig. 2A).

In the forced swim test (FST) in which a low immobility time is an indicator of the antidepressant-like response, a single intraperitoneal injection of ketamine significantly reduced the immobility of Sprague-Dawley rats (Fig. 2B). Compared with CA1 tissue from

saline-injected animals, ketamine increased GluA1 phosphorylation and abundance detected within 30 min after injection (Fig. 2C).

Ketamine-induced synaptic potentiation is independent of inhibitory synaptic input

Short-term synaptic disinhibition (reduction in inhibitory synaptic input) of hippocampal CA1 cells increases calcium influx through voltage-gated calcium channels and triggers the PKA signaling pathway (18). To test whether ketamine-induced potentiation of SC-CA1 transmission involved blocking inhibitory synaptic transmission, we pretreated hippocampal slices with picrotoxin and CGP52432 (CGP) [γ-aminobutyric acid type A ($GABA_A$) and $GABA_B$ receptor inhibitors, respectively], then applied ketamine, and measured SC-CA1 excitatory postsynaptic currents (EPSCs) recorded at the soma of CA1 pyramidal cells. When inhibitory transmission was blocked, bath application of ketamine potently and reversibly enhanced SC-CA1 EPSCs in a PKA-dependent manner (Fig. 3A). Paired-pulse ratios (PPRs) are measured as the amplitude ratio of the second to the first postsynaptic responses evoked by two successional stimuli. Ketamine significantly reduced PPRs of SC-CA1 EPSCs (Fig. 3B). One possible explanation for the reduced PPR is that presynaptic mechanisms participate in the action of ketamine. In addition, we observed that, in the presence of picrotoxin and CGP, the noncompetitive NMDAR antagonist MK-801 enhanced SC-CA1 transmission, mimicking the effect of ketamine (Fig. 3C). Furthermore, MK-801 completely blocked the effect of subsequent ketamine application on SC-CA1 EPSCs (Fig. 3C). This observation could be explained as blocking NMDARs is the initiating step for ketamine-induced potentiation of excitatory synaptic transmission at SC-CA1 synapses. Consistent with the lack of effect of blocking GABA transmission on ketamine responses, picrotoxin plus CGP did not occlude ketamine-induced increase in phosphorylation of GluA1 Ser^{845} and GluA1 abundance (Fig. 3D). Thus, it was unlikely that disinhibition was ultimately responsible for the enhancement in SC-CA1 transmission.

The antidepressant and electrophysiological effects of ketamine require GluA1 Ser^{845} phosphorylation

To confirm a role for phosphorylated Ser^{845} in the rapid antidepressant action of ketamine, we examined the effect of ketamine on hippocampal synaptic activity and behavior of GluA1 S845A knock-in mice. The GluA1 S845A knock-in mice have a mutation in the native gene encoding GluA1 (19), such that Ser^{845} was mutated to an alanine, which could not be phosphorylated by PKA. Ketamine failed to enhance SC-CA1 fEPSPs in slices from the mutant mice but strongly enhanced SC-CA1 fEPSPs in slices from wild-type littermate mice (Fig. 4A). Ketamine also failed to increase the membrane surface abundance of GluA1 in GluA1 S845A mice (Fig. 4B). Systemic administration of ketamine significantly reduced immobility of wild-type mice in the FST (Fig. 4C) but not in GluA1 S845A mice (Fig. 4D). These results indicated that GluA1 phosphorylation and potentiation of SC-CA1 synaptic transmission were not epiphenomena that occurred during ketamine application but were required for the fast-acting antidepressant responses of ketamine.

Ketamine enhances presynaptic excitatory transmission by inhibiting NMDARs

To examine the roles of pre- and postsynaptic NMDARs in the antidepressant actions of ketamine, we ablated NMDAR function specifically in CA3 cells (CA3-NR1 KO) and CA1

cells (CA1-NR1 KO) by knocking out the gene encoding the GluN1 (NR1) subunit of NMDAR, which prevents the production of any NMDARs (20, 21). CA1 cells are the postsynaptic neuron, and CA3 cells are the presynaptic neuron in forming SC-CA1 synapses. Ketamine enhanced SC-CA1 fEPSPs (Fig. 5A) and induced antidepressant responses in both novelty-suppressed feeding test and FST in CA1 CA1-NR1 KO mice (Fig. 5, C and E), indicating that ketamine's effects were not the result of inhibition of postsynaptic CA1 NMDARs. In contrast, ketamine neither enhanced SC-CA1 fEPSPs (Fig. 5B) nor exhibited antidepressant action in the two behavioral tests in CA3-NR1 KO mice (Fig. 5, D and F). Furthermore, dialyzing MK-801 through the patch pipette to only inhibit postsynaptic CA1 neurons in hippocampal preparations from wild-type mice did not occlude ketamine's effect on SC-CA1 EPSCs (fig. S1, A and B). Together, these results suggested that inhibition of NMDARs located on CA3 neurons but not on CA1 neurons is required for the ketamine-induced antidepressant responses and excitation.

Ketamine reduces HCN1 activity to elicit antidepressant effects

We next asked how presynaptic NMDAR inhibition enhanced SC-CA1 synaptic transmission and elicited the antidepressant actions of ketamine. A previous study reported that application of 2-amino-5-phosphonopentanoic acid (AP5), a competitive NMDAR antagonist, to hippocampal slices blocks glutamate-induced increase in the surface abundance of HCN1 channels, and NMDAR activation–induced calcium influx is required for the increase in HCN channel activity triggered by theta-burst stimulation (22, 23). HCN channels play important roles in synaptic transmission and plasticity. We therefore tested the impact of ketamine on the abundance and function of HCN1 channels in hippocampal CA1 stratum radiatum. We detected HCN1 channels in both isolated presynaptic active zones (enriched for syntaxin) and postsynaptic densities (enriched for PSD95) in this hippocampal subregion (fig. S2, A and B). We applied either ZD 7288 (ZD) or zatebradine, both of which are HCN channel blockers (24), in the presence of GABA receptor inhibitors to hippocampal slice preparations. Both ZD and zatebradine enhanced SC-CA1 EPSCs (Fig. 6, A and B). ZD also reduced PPR of SC-CA1 EPSCs (Fig. 6C). Furthermore, ZD perfusion completely occluded ketamine-induced potentiation on SC-CA1 EPSCs (Fig. 6A) and the ketamine-induced increases in GluA1 phosphorylation and abundance (Fig. 6D). In addition, ketamine failed to enhance SC-CA1 fEPSPs in slices from HCN1-knockout (HCN1-KO) mice and was ineffective in altering behavior in the sucrose preference test and the novelty-suppressed feeding test in these mutant mice (Fig. 6, E and F). In contrast, compared to the saline-injected group, ketamine increased immobility in the FST in HCN1-KO mice (Fig. 6F). These results suggested that HCN channels are involved in the action of ketamine on SC-CA1 synaptic transmission.

To isolate the roles of pre- and postsynaptic HCN channels in ketamine's action, we blocked postsynaptic HCN channels by dialyzing ZD into CA1 cells. We recorded SC-CA1 EPSCs and simultaneously monitored HCN channel–mediated current (I_h) during ZD dialysis. Intracellular ZD dialysis in the postsynaptic neuron did not increase the peak amplitude of SC-CA1 EPSCs, despite decreasing I_h and slowing the decay time of EPSCs, indicating that the postsynaptic HCN channels were blocked (Fig. 6G). Even after 1-hour ZD dialysis,

ketamine perfusion enhanced SC-CA1 EPSCs (Fig. 6H), consistent with a role of presynaptic HCN channels in ketamine's action.

DISCUSSION

Here, we provided evidence that GluA1 Ser^{845} phosphorylation and presynaptic NMDARs are required for the fast-acting antidepressant responses and electrophysiological effects of ketamine. This antidepressant action was absent in HCN1-KO mice, and inhibiting presynaptic, but not postsynaptic, HCN channels mimicked and occluded ketamine-induced potentiation of SC-CA1 fEPSPs, suggesting the involvement of presynaptic HCN channels in the fast-acting antidepressant actions of ketamine. Although it remains unclear how presynaptic NMDAR inhibition reduced the function of presynaptic HCN channels, previous studies reported that postsynaptic NMDAR inhibition reduced the amount of postsynaptic HCN channels (22, 23); HCN channels are present on specific axons and synaptic terminals in many brain regions, including the hippocampus, cerebellum, and cortex (25–28). Blocking presynaptic HCN channels increases the activity of the voltage-gated calcium channels $Ca_V2.3$, thus promoting glutamate release (27). Furthermore, the HCN channel blocker ZD increases the amplitude of SC-CA1 fEPSPs and EPSCs, and reduces PPR of fEPSPs, suggesting that HCN channels regulate SC-CA1 synaptic transmission through a presynaptic mechanism (29). Thus, we speculate that presynaptic NMDAR inhibition reduces presynaptic HCN channel function, leading to the promotion of glutamate release and enhancement of postsynaptic AMPA receptor phosphorylation, thus promoting surface insertion of AMPA receptors into the postsynaptic membrane.

Depending on the distribution and the background activity of the synapse, activation of presynaptic NMDARs may either decrease or enhance neurotransmitter release (30, 31). Both electrophysiological and imaging evidence supports the existence of presynaptic NMDARs at SC-CA1 synapses (31). All four GluN2 subunits (GluN2A, GluN2B, GluN2C, and GluN2D) and GluN3A subunit have been identified in presynaptic NMDARs (32). Among these receptor subtypes, GluN2C- or GluN2D-containing NMDARs exhibit less voltage-dependence (incomplete Mg^{2+} blockage) and are more sensitive to glutamate than postsynaptic NMDARs (31, 33). Compared with the effect of ketamine in Mg^{2+}-free solution, ketamine inhibition of NMDA receptors composed of GluN1 and GluN2A or GluN1 and GluN2B subunits decreases nearly 20-fold when applied in the presence of physiological concentration of Mg^{2+} (34). In this experiment, the channel subunits were transfected into embryonic kidney 293T mammalian cells and ketamine inhibition in the presence of Mg^{2+} was tested at a membrane voltage near the resting membrane potential. In contrast, changing the Mg^{2+} concentration only decreases the ketamine inhibition only ~threefold for NMDARs composed of GluN1 and GluN2C or GluN1 and GluN2D subunits (34). Thus, presynaptic NMDA receptors with the GluN2C or GluN2D subunits may be much more sensitive to ketamine in the physiological concentration of Mg^{2+} than are postsynaptic NMDA receptors, which have a different subunit composition.

Another study showed that the metabolites of ketamine also exhibit antidepressant-like actions (35). Because the brain is incapable of metabolizing ketamine (36), the responses that we observed here for acutely prepared brain slices were likely mediated by ketamine

itself. A study by Autry *et al*. (8) reported thatMK-801 decreased immobility of animals in the FST at 3 hours after administration. Another NMDAR antagonist, carboxypiperazin-4-yl-propyl-1-phosphonic acid (CPP), also produced this effect, which lasted for 24 hours after injection (8). Furthermore, none of these NMDAR antagonists (ketamine, MK-801, and CPP) altered locomotor activity of the tested animals (8). Zanos and colleagues reported that blockade of NMDARs at the glycine$_B$ co-agonist site induced a rapid antidepressant response, which was not associated with psychotomimetic effects and lasted at least for 7 days (37). In contrast, memantine, another noncompetitive NMDA antagonist that binds the same binding site (Mg^{2+} site) inside the ion channel as MK-801 binds, has not been shown to exhibit clear antidepressant action. These observations indicate that NMDAR inhibition can induce rapid, safe, and sustained antidepressant responses and that a subtle variation in the property of antagonism, such where within the channel the compound binds and blocks, and how long the molecule remains within the channel (trapping time), may alter the effectiveness of antidepressant actions of NMDAR antagonists.

Consistent with structural variation affecting antidepressant action, (*R,S*)-d$_2$-KET (ketamine deuterated at the C6 position) lacks antidepressant action in the FST and animals with "learned helplessness" (35). The subtle modification of the structure of ketamine may change its trapping time or off-rate inside the NMDA channels and thus potently affects the effectiveness of antidepressant responses, although the affinity to NMDAR may not be substantially altered. Furthermore, (2R,6R)–hydroxynorketamine (HNK), the major effective metabolite of ketamine in antidepressant responses, increased the frequency of spontaneous EPSCs recorded at CA1 stratum radiatum interneuron and enhanced the slope of SC-CA1 fEPSPs for about sixfold in the presence of the NMDAR antagonist AP5 (35). These results suggest that (2R,6R)-HNK may potentiate excitatory synaptic transmission by enhancing presynaptic glutamate release. However, the authors also observed that (2R,6R)-HNK significantly decreased eukaryotic elongation factor 2 phosphorylation, an effect caused by blockade of postsynaptic NMDARs in unstimulated neurons at rest (8, 38). Thus, the connections between these observations as well as the cellular signaling induced by the metabolite of ketamine and the ketamine-induced antidepressant responses remain elusive and require investigation.

We have provided evidence for the essential roles of presynaptic NMDARs, presynaptic HCN channels, and postsynaptic AMPA receptor GluA1 phosphorylation in the fast-acting antidepressant actions of ketamine. This knowledge advances our understanding of the cellular mechanisms underlying ketamine's antidepressant effects and opens a potential avenue for developing new antidepressant drugs to provide a safer and more expedient therapy for MDD.

MATERIALS AND METHODS

Animals

Sprague-Dawley rats were purchased from Harlan Laboratories (Indianapolis, IN).HCN1-KOmice were purchased from The Jackson Laboratory (#16566).As reported by others (20), conditional mutant CA1 cell-specific NR1-KO mice were generated by crossing NR1^{flox} mice (The Jackson Laboratory, #005246) with CaMKIIα-Cre T29-1 transgenic mice (The

Jackson Laboratory, #005359). Conditional mutant CA3 cell-specific NR1-KO mice were obtained by breeding $NR1^{flox}$ mice with G32-4 Cre transgenic mice (The Jackson Laboratory, #00647) (21). Both male and female rats or mice used for tissue preparation or behavioral tests in this study were 8- to 14-week old. All experimental procedures involving animals were performed in accordance with National Institutes of Health (NIH) Guidelines for the Care and Use of Laboratory Animals and were approved by the Animal Care Committee of Southern Illinois University, Carbondale.

Hippocampal slice preparation

This method was described in detail in our previous publication (39). Briefly, rats or mice were killed by decapitation after sedation with Euthasol solution [containing sodium pentobarbital (390 mg/ml) and phenytoin sodium (50 mg/ml); 0.5 ml/kg, i.p.; Henry Schein). Brains were rapidly removed, and hippocampal dissection was done in ice-cold ACSF (124 mM NaCl, 3 mM KCl, 1.25 mM NaH_2PO_4, 1.0 mM $MgCl_2$, 2.5 mM $CaCl_2$, 26 mM $NaHCO_3$, and 10 mM glucose) bubbled with 95% O_2/5% CO_2. Isolated hippocampi were sectioned into 400 μM slices using a vibratome (VT1000 S, Leica), kept in a holding chamber at room temperature (20° to 22°C) at the interface of ACSF, and humidified in 95% O_2/5% CO_2 for minimally1 hour.

Extracellular field potential recordings

After incubation, hippocampal slices were transferred to a submersion-type recording chamber and perfused at room temperature with ACSF (flow rate = 1 to 2 ml/min). Concentric bipolar tungsten electrodes were placed in stratum radiatum of area CA1 to stimulate Schaffer collateral afferents. Extracellular recording pipettes (1 to 2 megohms) were filled with ACSF and placed 100 to 150 μm from the stimulating electrodes in stratum radiatum. Stimuli (100-μs duration) were delivered at 0.05 Hz. The stimulus intensity was set at 150% of threshold intensity, resulting in a field EPSPs (fEPSPs) of 0.1 to 0.2 mV. All compounds were applied by perfusion. Field EPSPs were recorded using Axoclamp 2B or Axopatch 200B amplifier (Molecular Devices); signals were amplified 100× and filtered at 10 kHz before digitization using a Digidata 1440A A/D converter (Molecular Devices).

Whole-cell patch-clamp recordings

Whole-cell voltage clamp recordings were obtained with patch pipettes filled with 135 mM $CsCH_3SO_3$, 10 mM Hepes, 10 mM NaCl, 1 mM $MgCl_2$, 0.1 mM BAPTA [K_4 1,2-bis(2-aminophenoxy)ethane-*N,N,N′,N′*-tetraacetic acid], 2 mM Mg^{2+}–ATP, and 10 mM phosphocreatine, 5 mM QX-314 adjusted to pH 7.3 with CsOH, and with final osmolarity of about 305. In some experiments, picrotoxin (100 μM) and CGP (4 μM) were included in ACSF to block $GABA_A$ and $GABA_B$ receptors, respectively. In these experiments, area CA3 and the dentate gyrus were removed from the slices to prevent spontaneous epileptiform discharges. Hippocampal CA1 pyramidal cells were visualized with a 40× water-immersion lens and illuminated with near-infrared (IR) light; images were detected with an IR-sensitive charge-coupled device camera. Electrode resistances in the bath were 3 to 6 megohms, and series resistances of <40 megohms were accepted. Data were collected using Multiclamp 700B or Axonpatch 200B amplifier (Molecular Devices), low-pass–filtered at 2 kHz, and digitized at 5 kHz using a Digidata 1440A A/D converter and Clampex 10.3 software

(Molecular Devices). Paired-pulse facilitation of EPSCs was evaluated by paired-pulse stimulation at an interstimulus interval of 75 ms during the baseline conditions and after drug application. PPRs were calculated as amplitude of EPSC2/amplitude of EPSC1. H currents were recorded in response to 3-s voltage steps to between −60 and −130 mV in 10-mV increments from a holding potential of −60 mV.

Forced swim test

In the pretest session [24 hours before the end of chronic mild stress (CMS)], rats or mice were placed into a water-filled Plexiglas cylinder (10,000-ml cylinder filled with 6000-ml water for rats and 4000-ml cylinder filled with 3000-ml water for mice; water temperature, 20° to 22°C) for 15 min. The animal was then removed, dried with a towel, and returned to its home cage. The water in the cylinders was changed between subjects. A test session was performed 24 hours after pretest. The test session, also performed for 15 min, was recorded by a video camera positioned on the side of the cylinder to evaluate locomotor activity. The first 5 min of the test session was analyzed and scored by an observer blind to group assignment. A decrease in immobility time (that is, more swimming/struggling while in the water) is suggestive of an antidepressant-like response.

Sucrose preference test

To accustom mice to the taste of sucrose, ad libitum water was replaced with a 0.5% sucrose solution for 3 days, and then tap water was returned on the last day of CMS procedure. On the day of test, mice were provided with one bottle of water and one bottle of 0.5% sucrose-containing water for the 48-hour test period. The position of the bottles was reversed after 24 hours during the test. The consumption of water and sucrose was measured by weighing the bottles. Preference for sucrose was calculated as a percentage of the sucrose-containing solution consumed divided by the total amount of liquid intake.

Membrane surface protein biotinylation

Hippocampal slices, prepared as described above, were maintained at room temperature for at least 1 hour. Area CA1 wedges were dissected from the slices and then transferred to ice-cold ACSF (bubbled with 95% O_2/5% CO_2) containing sulfosuccinimidyl-2-(biotinamido)ethyl-1,3-dithiopropionate (1 mg/ml; sulfo-NHS-SS-biotin; Fisher Scientific) for 1 hour to biotinylate surface proteins. Excess biotin was then removed by washing the slices three times with ice-cold ACSF to eliminate free sulfo-NHS-SS-biotin. Eight to 12 hippocampal CA1 wedges were pooled and homogenized in 600 μl of modified radioimmunoprecipitation assay buffer (Fisher Scientific) containing 150 mM NaCl, 20 mM Hepes, 1% Triton X-100, 0.5% SDS, and 2 mM EDTA (pH 7.4), and supplemented with a cocktail of protease and phosphatase inhibitors. Samples were homogenized for 30 s and placed on ice under agitation for 1 hour. Homogenates (total fractions) were collected, and cell debris was removed by centrifugation at 13,000 rpm for 10 min at 4°C. Supernatants were collected, and a small fraction (20 μg) was removed for total protein measurement by Western blotting. For surface protein detection, the supernatants were incubated overnight at 4°C with prewashed NeutrAvidin agarose beads (50 μl, Fisher Scientific) to capture biotinylated proteins. Beads were collected by a brief centrifugation, and supernatants were discarded. Sedimented beads were washed three times in phosphate buffered saline, and

biotinylated proteins were finally eluted with loading buffer (boiled at 100°C for 5 min). Biotinylated fractions were collected, and levels of surface proteins were estimated by Western blotting. Levels of surface and total GluA1 were expressed as a ratio to actin, which was only detected in total proteins.

Western blot analysis

Supernatant containing the total proteins (added with loading buffer, boiled at 100°C for 5 min) or biotinylated proteins was loaded into 7.5% bis-tris gel (Bio-Rad). After running in 1× NuPAGE MOPS SDS buffer (Fisher Scientific), the gel was transferred onto polyvinylidene difluoride membranes in 1× NuPAGE transfer buffer (in 20% methanol, w/v). The membrane was blocked with 5% nonfat dry milk (w/v) in buffer containing 1 M tris-buffered saline and 0.1% Tween 20 (v/v) (TBS-Tween), and incubated with primary antibodies against S845-phosphorylated GluA1 (1:1000; Cell Signaling Technology, #13185) (39) overnight at 4°C. After three rinses in TBS-Tween, the membrane was incubated for 1 hour at room temperature in horseradish peroxidase–conjugated goat anti-rabbit immunoglobulin G (1:3000; Fisher Scientific, #31462). The immunoblot was developed with enhanced chemiluminescence (Fisher Scientific). Membranes were then stripped, blocked, and reprobed with antibodies against GluA1 (0.5 μg/ml; Thermo Fisher Scientific, PA1-37776) (40) or β-actin (1:2000; Cell Signaling Technology, #4967) (41). Levels of phosphorylation, expressed as the ratio of phosphospecific intensity divided by total protein intensity and computed with ImageJ, were used for statistical analysis. For display purposes, blots were cropped, and brightness and contrast were adjusted globally using Photoshop (www.adobe.com).

Detecting HCN1 expression in presynaptic active zone and postsynaptic density

As previous studies reported (42, 43), slice wedges of CA1 stratum radiatum were isolated from acutely prepared hippocampal slices from two to three adult Sprague-Dawley rats. Slice wedges were homogenized, and the resultant homogenate was centrifuged to remove nuclei and cellular debris. Synaptosomal fractions were purified by centrifugation in Percoll-sucrose density gradient. The purified synaptosome was centrifuged, resuspended with ice cold 0.1 mM $CaCl_2$, and incubated with 2× solubilization buffer [2% Triton X-100, 40 mM tris (pH 6.0)] to isolate synaptic junction (containing presynaptic active zone and postsynaptic density). After centrifugation, synaptic junction was incubated in 1× solubilization buffer with pH 8.0. Postsynaptic density (in the pellet) and presynaptic active zone (in the supernatant) were isolated by centrifugation at 40,000 rpm. Pre- and postsynaptic HCN channels were probed by HCN1 primary antibodies (raised from rabbit; Alomone Labs, #APC-056) (44) in isolated presynaptic active zone and postsynaptic density, respectively, in Western blot analysis, and syntaxin (Abcam, #2365) and PSD95 (Millipore, #AB9708) (45) were used as marker proteins for pre- and postsynaptic labeling, respectively.

Statistical analysis

All data are presented as means ± SEM. Paired or unpaired *t* tests, or one-way repeated ANOVA followed by Bonferroni or Tukey's post hoc tests, were used to determine statistical significance between groups. *P* values of ≤0.05 were regarded as significant.

Supplementary Material

Refer to Web version on PubMed Central for supplementary material.

Acknowledgments

We thank G. Rose and P. Jensik for reading and revising the manuscript. We thank P. Patrylo for technical support. **Funding:** This study was supported by the National Institute of Mental Health (NIMH) R01 (NIHMH086828), Southern Illinois University School of Medicine startup funds (501871), National Natural Science Foundation of China (81271488 and 81671339), Science and Technology Program of Guangzhou, China (2014Y2-00096), Pearl River Scholar Program by Guangdong Province, China, Foundation for High-level Talents in Higher Education of Guangdong, China (310109-012), and Research Project for Colleges and Universities in Guangzhou (12A002S).

References

1. Kessler D, Sharp D, Lewis G. Screening for depression in primary care. Br. J. Gen. Pract. 2005; 55:659–660. [PubMed: 16176729]
2. Belmaker RH, Agam G. Major depressive disorder. N. Engl. J. Med. 2008; 358:55–68. [PubMed: 18172175]
3. León I, Cimadevilla JM, Tascón L. Developmental gender differences in children in a virtual spatial memory task. Neuropsychology. 2014; 28:485–495. [PubMed: 24588700]
4. Berman RM, Cappiello A, Anand A, Oren DA, Heninger GR, Charney DS, Krystal JH. Antidepressant effects of ketamine in depressed patients. Biol. Psychiatry. 2000; 47:351–354. [PubMed: 10686270]
5. Monteggia LM, Zarate C Jr. Antidepressant actions of ketamine: From molecular mechanisms to clinical practice. Curr. Opin. Neurobiol. 2015; 30:139–143. [PubMed: 25562451]
6. Kishimoto T, Chawla JM, Hagi K, Zarate CA. Single-dose infusion ketamine and nonketamine *N*-methyl-d-aspartate receptor antagonists for unipolar and bipolar depression: A meta-analysis of efficacy, safety and time trajectories. Psychol. Med. 2016; 46:1459–1472. [PubMed: 26867988]
7. Browne CA, Lucki I. Antidepressant effects of ketamine: Mechanisms underlying fast-acting novel antidepressants. Front. Pharmacol. 2013; 4:161. [PubMed: 24409146]
8. Autry AE, Adachi M, Nosyreva E, Na ES, Los MF, Cheng P-f, Kavalali ET, Monteggia LM. NMDA receptor blockade at rest triggers rapid behavioural antidepressant responses. Nature. 2011; 475:91–95. [PubMed: 21677641]
9. Li N, Lee B, Liu R-J, Banasr M, Dwyer JM, Iwata M, Li X-Y, Aghajanian G, Duman RS. mTOR-dependent synapse formation underlies the rapid antidepressant effects of NMDA antagonists. Science. 2010; 329:959–964. [PubMed: 20724638]
10. Kavalali ET, Monteggia LM. How does ketamine elicit a rapid antidepressant response? Curr. Opin. Pharmacol. 2015; 20:35–39. [PubMed: 25462290]
11. Airan RD, Meltzer LA, Roy M, Gong Y, Chen H, Deisseroth K. High-speed imaging reveals neurophysiological links to behavior in an animal model of depression. Science. 2007; 317:819–823. [PubMed: 17615305]
12. MacQueen GM, Campbell S, McEwen BS, Macdonald K, Amano S, Joffe RT, Nahmias C, Young LT. Course of illness, hippocampal function, and hippocampal volume in major depression. Proc. Natl. Acad. Sci. U.S.A. 2003; 100:1387–1392. [PubMed: 12552118]
13. Miller BR, Hen R. The current state of the neurogenic theory of depression and anxiety. Curr. Opin. Neurobiol. 2015; 30:51–58. [PubMed: 25240202]
14. Derkach VA, Oh MC, Guire ES, Soderling TR. Regulatory mechanisms of AMPA receptors in synaptic plasticity. Nat. Rev. Neurosci. 2007; 8:101–113. [PubMed: 17237803]
15. George MS, Abbott LF, Siegelbaum SA. HCN hyperpolarization-activated cation channels inhibit EPSPs by interactions with M-type K^+ channels. Nat. Neurosci. 2009; 12:577–584. [PubMed: 19363490]
16. Li J, Chen F-f, Chen X-d, Zhou C. Inhibition of HCN1 channels by ketamine accounts for its antidepressant actions. Sichuan Daxue Xuebao Yixueban. 2014; 45:888–892.

17. Roche KW, O'Brien RJ, Mammen AL, Bernhardt J, Huganir RL. Characterization of multiple phosphorylation sites on the AMPA receptor GluR1 subunit. Neuron. 1996; 16:1179–1188. [PubMed: 8663994]
18. Hsu K-S, Ho W-C, Huang C-C, Tsai J-J. Prior short-term synaptic disinhibition facilitates long-term potentiation and suppresses long-term depression at CA1 hippocampal synapses. Eur. J. Neurosci. 1999; 11:4059–4069. [PubMed: 10583494]
19. Lee H, Takamiya K, Han J, Man H, Kim C, Rumbaugh G, Yu S, Ding L, He C, Petralia RS, Wenthold RJ, Gallagher M, Huganir RL. Phosphorylation of the AMPA receptor GluR1 subunit is required for synaptic plasticity and retention of spatial memory. Cell. 2003; 112:631–643. [PubMed: 12628184]
20. Tsien JZ, Huerta PT, Tonegawa S. The essential role of hippocampal CA1 NMDA receptor–dependent synaptic plasticity in spatial memory. Cell. 1996; 87:1327–1338. [PubMed: 8980238]
21. Nakazawa K, Quirk MC, Chitwood RA, Watanabe M, Yeckel MF, Sun LD, Kato A, Carr CA, Johnston D, Wilson MA, Tonegawa S. Requirement for hippocampal CA3 NMDA receptors in associative memory recall. Science. 2002; 297:211–218. [PubMed: 12040087]
22. Fan Y, Fricker D, Brager DH, Chen X, Lu H-C, Chitwood RA, Johnston D. Activity-dependent decrease of excitability in rat hippocampal neurons through increases in I_h. Nat. Neurosci. 2005; 8:1542–1551. [PubMed: 16234810]
23. Noam Y, Zha Q, Phan L, Wu R-L, Chetkovich DM, Wadman WJ, Baram TZ. Trafficking and surface expression of hyperpolarization-activated cyclic nucleotide-gated channels in hippocampal neurons. J. Biol. Chem. 2010; 285:14724–14736. [PubMed: 20215108]
24. Gill CH, Randall A, Bates SA, Hill K, Owen D, Larkman PM, Cairns W, Yusaf SP, Murdock PR, Strijbos PJLM, Powell AJ, Benham CD, Davies CH. Characterization of the human HCN1 channel and its inhibition by capsazepine. Br. J. Pharmacol. 2004; 143:411–421. [PubMed: 15351778]
25. Zong X, Eckert C, Yuan H, Wahl-Schott C, Abicht H, Fang L, Li R, Mistrik P, Gerstner A, Much B, Baumann L, Michalakis S, Zeng R, Chen Z, Biel M. A novel mechanism of modulation of hyperpolarization-activated cyclic nucleotide-gated channels by Src kinase. J. Biol. Chem. 2005; 280:34224–34232. [PubMed: 16079136]
26. Zhou W, Zhang L, Guoxiang X, Mojsilovic-Petrovic J, Takamaya K, Sattler R, Huganir R, Kalb R. GluR1 controls dendrite growth through its binding partner, SAP97. J. Neurosci. 2008; 28:10220–10233. [PubMed: 18842882]
27. Huang Z, Lujan R, Kadurin I, Uebele VN, Renger JJ, Dolphin AC, Shah MM. Presynaptic HCN1 channels regulate $Ca_V3.2$ activity and neurotransmission at select cortical synapses. Nat. Neurosci. 2011; 14:478–486. [PubMed: 21358644]
28. Notomi T, Shigemoto R. Immunohistochemical localization of I_h channel subunits, HCN1–4, in the rat brain. J. Comp. Neurol. 2004; 471:241–276. [PubMed: 14991560]
29. Tokay T, Rohde M, Krabbe S, Rehberg M, Bender RA, Köhling R, Kirschstein T. HCN1 channels constrain DHPG-induced LTD at hippocampal Schaffer collateral-CA1 synapses. Learn. Mem. 2009; 16:769–776. [PubMed: 19940037]
30. Bardoni R, Torsney C, Tong CK, Prandini M, MacDermott AB. Presynaptic NMDA receptors modulate glutamate release from primary sensory neurons in rat spinal cord dorsal horn. J. Neurosci. 2004; 24:2774–2781. [PubMed: 15028770]
31. Bouvier G, Bidoret C, Casado M, Paoletti P. Presynaptic NMDA receptors: Roles and rules. Neuroscience. 2015; 311:322–340. [PubMed: 26597763]
32. Larsen RS, Corlew RJ, Henson MA, Roberts AC, Mishina M, Watanabe M, Lipton SA, Nakanishi N, Pérez-Otaño I, Weinberg RJ, Philpot BD. NR3A-containing NMDARs promote neurotransmitter release and spike timing–dependent plasticity. Nat. Neurosci. 2011; 14:338–344. [PubMed: 21297630]
33. Siegler Retchless B, Gao W, Johnson JW. A single GluN2 subunit residue controls NMDA receptor channel properties via intersubunit interaction. Nat. Neurosci. 2012; 15:406–413. [PubMed: 22246434]
34. Kotermanski SE, Johnson JW. Mg^{2+} imparts NMDA receptor subtype selectivity to the Alzheimer's drug memantine. J. Neurosci. 2009; 29:2774–2779. [PubMed: 19261873]

35. Zanos P, Moaddel R, Morris PJ, Georgiou P, Fischell J, Elmer GI, Alkondon M, Yuan P, Pribut HJ, Singh NS, Dossou KSS, Fang Y, Huang X-P, Mayo CL, Wainer IW, Albuquerque EX, Thompson SM, Thomas CJ, Zarate CA Jr, Gould TD. NMDAR inhibition-independent antidepressant actions of ketamine metabolites. Nature. 2016; 533:481–486. [PubMed: 27144355]
36. Cohen ML, Chan SL, Way WL, Trevor AJ. Distribution in the brain and metabolism of ketamine in the rat after intravenous administration. Anesthesiology. 1973; 39:370–376. [PubMed: 4758343]
37. Zanos P, Piantadosi SC, Wu H-Q, Pribut HJ, Dell MJ, Can A, Snodgrass HR, Zarate CA, Schwarcz R, Gould TD. The Prodrug 4-chlorokynurenine causes ketamine-like antidepressant effects, but not side effects, by NMDA/glycine$_B$-site inhibition. J. Pharmacol. Exp. Ther. 2015; 355:76–85. [PubMed: 26265321]
38. Nosyreva E, Szabla K, Autry AE, Ryazanov AG, Monteggia LM, Kavalali ET. Acute suppression of spontaneous neurotransmission drives synaptic potentiation. J. Neurosci. 2013; 33:6990–7002. [PubMed: 23595756]
39. Cai X, Kallarackal AJ, Kvarta MD, Goluskin S, Gaylor K, Bailey AM, Lee H-K, Huganir RL, Thompson SM. Local potentiation of excitatory synapses by serotonin and its alteration in rodent models of depression. Nat. Neurosci. 2013; 16:464–472. [PubMed: 23502536]
40. Li X, DeJoseph MR, Urban JH, Bahi A, Dreyer J-L, Meredith GE, Ford KA, Ferrario CR, Loweth JA, Wolf ME. Different roles of BDNF in nucleus accumbens core versus shell during the incubation of cue-induced cocaine craving and its long-term maintenance. J. Neurosci. 2013; 33:1130–1142. [PubMed: 23325250]
41. Aghajanian H, Cho YK, Manderfield LJ, Herling MR, Gupta M, Ho VC, Li L, Degenhardt K, Aharonov A, Tzahor E, Epstein JA. Coronary vasculature patterning requires a novel endothelial ErbB2 holoreceptor. Nat. Commun. 2016; 7:12038. [PubMed: 27356767]
42. Feligioni M, Holman D, Haglerod C, Davanger S, Henley JM. Ultrastructural localisation and differential agonist-induced regulation of AMPA and kainate receptors present at the presynaptic active zone and postsynaptic density. J. Neurochem. 2006; 99:549–560. [PubMed: 16903873]
43. Phillips GR, Huang JK, Wang Y, Tanaka H, Shapiro L, Zhang W, Shan W-S, Arndt K, Frank M, Gordon RE, Gawinowicz MA, Zhao Y, Colman DR. The presynaptic particle web: Ultrastructure, composition, dissolution, and reconstitution. Neuron. 2001; 32:63–77. [PubMed: 11604139]
44. Stieber J, Stöckl G, Herrmann S, Hassfurth B, Hofmann F. Functional expression of the human HCN3 channel. J. Biol. Chem. 2005; 280:34635–34643. [PubMed: 16043489]
45. Rodenas-Ruano A, Chávez AE, Cossio MJ, Castillo PE, Zukin RS. REST-dependent epigenetic remodeling promotes the developmental switch in synaptic NMDA receptors. Nat. Neurosci. 2012; 15:1382–1390. [PubMed: 22960932]

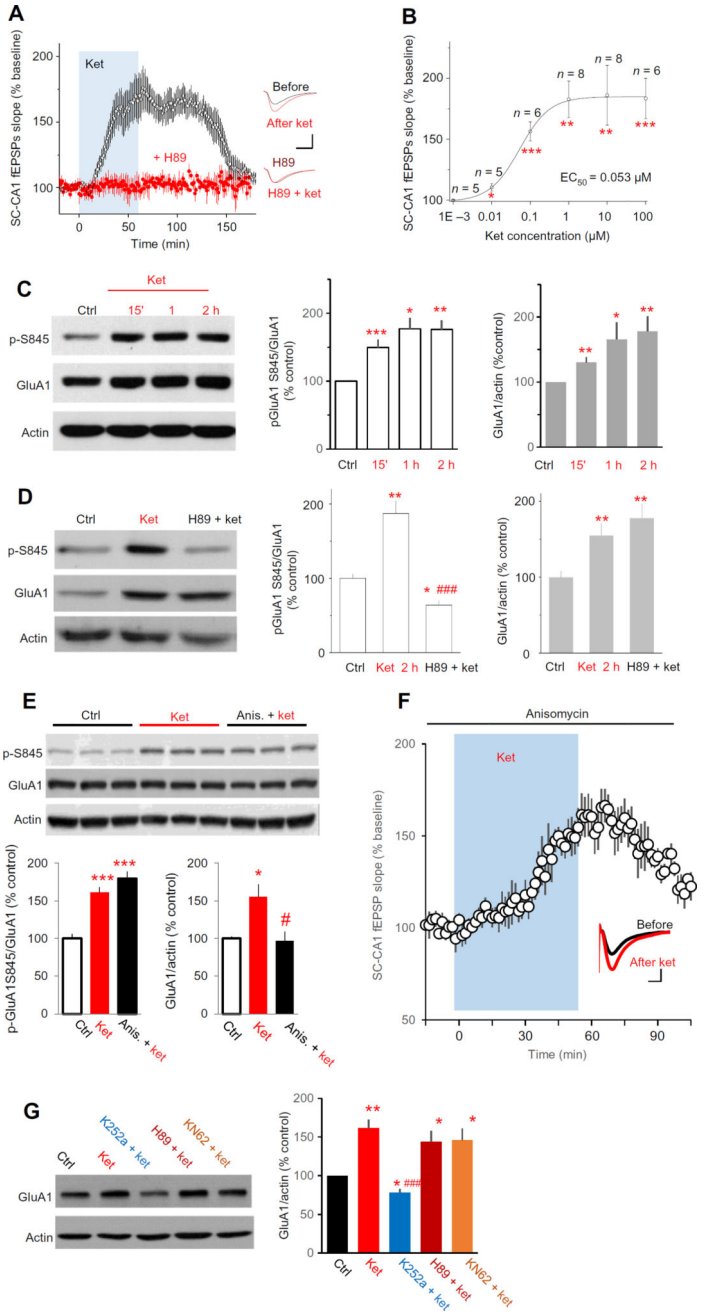

Fig. 1. Ketamine increases phosphorylation of GluA1 at hippocampal CA1 and enhances SC-CA1 synaptic transmission through a PKA-dependent mechanism

(**A**) Effect of ketamine (ket) on SC-CA1 fEPSPs, recorded in the stratum radiatum of CA1 in acutely prepared rat hippocampal slices. Ket (20 μM) was applied to the bath in the presence or absence of H89 (10 μM, PKA inhibitor), which was preapplied for 1 hour and maintained throughout the experiment. Left: Data are presented as the time course of SC-CA1 fEPSPs slope before and after ket application (blue shading) in control artificial cerebrospinal fluid (ACSF) or in the presence of H89 (ket in control ACSF: 175 ± 7.2% of baseline at 51 to 60 min after ket application; $n = 13$ from 10 animals, $P = 0.00012$, paired t test; H89: 105 ± 5.4% of baseline; $n = 6$ from four animals, $P = 0.69$, paired t test). Right: Representative

fEPSP averages before and after ket application. Drug responses were measured at 51 to 60 min after applied for all electrophysiological experiments in this paper. (**B**) Dose-response relationship of ket and the slope of SC-CA1 fEPSPs plotted with a best-fit sigmoidal function. Concentrations on the abscissa are $\log_{10}$ coordinates. The value of n presents the number of slices recorded. *$P < 0.05$, **$P < 0.01$, and ***$P < 0.001$ compared to control. (**C**) Effect of ket on GluA1 Ser^{845} phosphorylation and GluA1 abundance. Representative Western blots and data summary of six independent experiments showing that phosphorylation of GluA1 Ser^{845} and expression of total GluA1 were both significantly increased after ket bath application. (**D**) Effect of PKA inhibition on ket-induced increase in GluA1 Ser^{845} phosphorylation and GluA1 abundance. Rat hippocampal slices were exposed to saline (Ctrl) and ket (20 μM) in the presence or absence of H89 (10 μM). Top: Representative Western blots. Bottom: Data quantified from six independent Western blot experiments. (**E**) Effect of ket on GluA1 abundance and GluA1 Ser^{845} phosphorylation in the presence of a protein synthesis inhibitor. Rat hippocampal slices were exposed to saline and ket (20 μM) in the presence or absence of anisomycin (20 μM). Top: Representative Western blots. Bottom: Data quantified from four independent Western blot experiments [GluA1 Ser^{845} phosphorylation: $F_{2,9} = 39.52$, $P < 0.0001$, analysis of variance (ANOVA); $P = 0.245$, Bonferroni post hoc test between ket group and anisomycin plus ket group; total GluA1: $F_{2,9} = 7.635$, $P = 0.0115$, ANOVA; $P = 0.021$ for Bonferroni post hoc test between ket group and anisomycin plus ket group]. *$P < 0.05$ and ***$P < 0.001$ compared to control, and $^{\#}P < 0.05$ compared to ket alone, Bonferroni post hoc test after ANOVA. (**F**) Effect of ket on SC-CA1 fEPSPs in the presence of a protein synthesis inhibitor. Rat hippocampal slices were preexposed to anisomycin (20 μM) for 30 min and then ket (20 μM, blue shading). Graph shows SC-CA1 fEPSP slope, and inset shows representative traces before and after ket application. $n = 6$ slices from four rats; $P < 0.05$, paired t test. Scale bar, 5 ms/0.2 mV. (**G**) Effect of Trk, PKA, and CaMKII inhibition on the ket-induced increase in GluA1 abundance. Acutely prepared rat hippocampal slices were incubated with ACSF (Ctrl) or ket (20 μM), or ket and K252a (0.1 μM, Trk inhibitor), H89 (10 μM, PKA inhibitor), or KN62 (5 μM, CaMKII inhibitor). Left: Representative Western blots. Right: Data quantified from five independent Western blot experiments. $F_{4,16} = 6.587$, $P = 0.0025$, ANOVA. *$P < 0.05$ and **$P < 0.01$ compared to control, and $^{\#\#\#}P < 0.001$ compared to ket alone, Tukey's post hoc test after ANOVA.

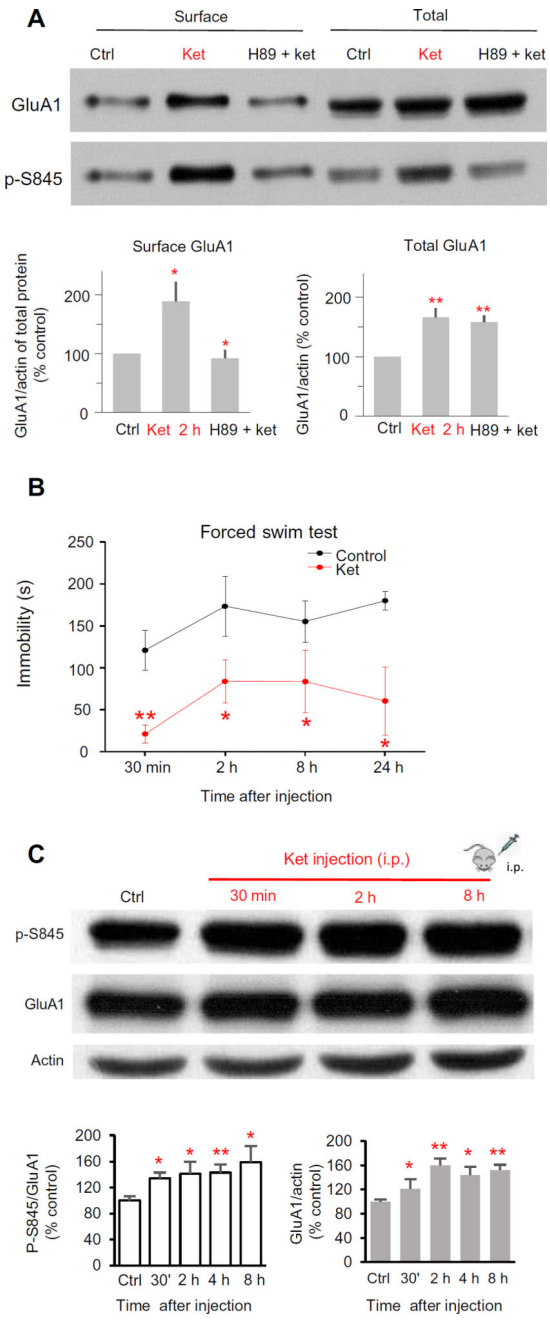

Fig. 2. Ket increases the abundance of GluA1 at the cell surface in PKA-dependent manner

(**A**) Effect of ket on the abundance of GluA1 and phosphorylated GluA1 Ser^{845} (p-S845) at the cell surface. Acutely prepared rat hippocampal slices were incubated with ACSF, ket (20 μM), or H89 (10 μM) and ket (20 μM) (H89 + ket) for 2 hours before biotinylation assays were performed. Top: Representative blots. Bottom: Quantified data from six independent membrane protein biotinylation experiments (surface GluA1: 189 ± 33.3% of control for ket; 92 ± 13.6% for H89 plus ket; $F_{2,18} = 6.68$, $P = 0.0068$, ANOVA; $P = 0.012$, Bonferroni post hoc test between the two groups; total GluA1: 166 ± 15.4% for ket; 159 ± 10.8% for H89 plus ket; $F_{2,15} = 9.59$, $P = 0.0021$, ANOVA; $P > 0.99$, Bonferroni post hoc test, H89

plus ket versus control). (**B**) Effect of a single ket injection on animal behavior in the forced swim. Rats were subjected to the FST 30 min and 2, 8, and 24 hours after saline (control) or ket injection [10 mg/kg, intraperitoneally (i.p.)]. $n = 5$ animals in each group; $^{*}P < 0.05$; $^{**}P < 0.01$, control versus ket, *t* test. (**C**) Effect of a single ket injection on GluA1 Ser^{845} phosphorylation and total GluA1 abundance in CA1 area tissue wedges from rat hippocampal slices. Top: Representative Western blots. Bottom: Quantified data from $n = 8$ rats for each time point. $^{*}P < 0.05$; $^{**}P < 0.01$, compared to saline injection group.

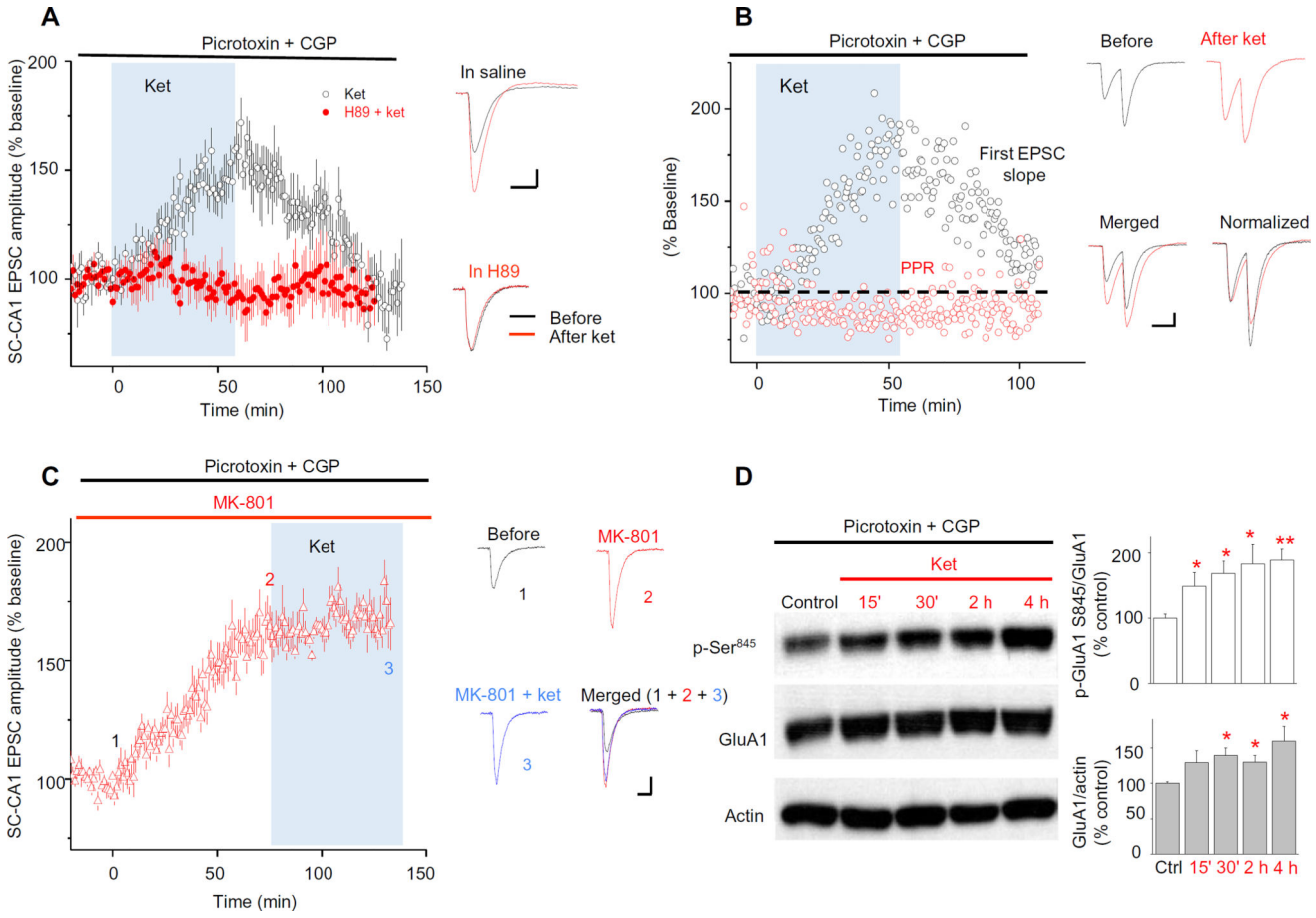

Fig. 3. Ket alters presynaptic transmission independently of GABA inhibitory input

(**A**) Effect of PKA inhibition and GABAergic input on the action of ket on SC-CA1 EPSCs recorded from CA1 neurons in hippocampal slices from rats. Hippocampal slices were pretreated for 30 min with picrotoxin (100 μM) and CGP (4 μM) to inhibit GABAergic signaling. Blue shading indicates the period of exposure to ket (20 μM) in the presence or absence of H89 (PKA inhibitor, 10 μM). All drugs were applied to the bath solution. Left: Data are presented as the EPSC amplitude normalized to the baseline before ket application (ket: 163 ± 8.3%of baseline, n=11, $P < 0.001$, paired t test). Right: Representative traces before and after ket in the absence (top) or presence (bottom) of H89. Scale bar, 40 ms/30 pA. (**B**) Effect of ket on SC-CA1 EPSCs and PPR of EPSCs in the presence of picrotoxin and CGP. Data were obtained using the same concentrations of drugs applied as in (A). Left: Representative data from a single-cell recording are presented as the ratio of the second EPSC amplitude to the first EPSC normalized to the baseline before ket application. Ket significantly decreased PPR of EPSCs: 81.3 ± 4.1% of baseline; n = 12 slices, $P < 0.0001$, paired t test. Right: Representative traces before and after ket application as well as merged and normalized (to before ket) traces. Scale bar, 40 ms/30 pA. (**C**) Effect of inhibition of NMDARs by MK-801 on SC-CA1 EPSCs and the effect to ket. Slices were pretreated by bath application for 1 hour with picrotoxin (100 μM) and CGP (CPG, 4 μM). Blue shading indicates the period of exposure to ket (20 μM). Left: Data are presented as the EPSC amplitude normalized to the baseline beforeMK-801 application (afterMK-801: 165 ± 6.0%

of baseline; after MK-801 plus ket: 171 ± 20.2% of baseline; $F_{2,23}$=6.87, P = 0.0046, ANOVA; P > 0.99 between the two groups, Bonferroni post hoc test). Right: Representative traces. (1) Baseline in picrotoxin and CGP, (2) after MK-801 application, and (3) after ket application in continuous MK-801 treatment. Scale bar, 40 ms/30 pA. (**D**) Effect of ket on GluA1 abundance and phosphorylation when GABAergic inhibition is blocked. Rat hippocampal slices were treated with drugs at the same concentrations as in (A). Representative blots are shown along with normalized quantified data from five independent experiments. *P < 0.05, **P < 0.01, ***P < 0.001 compared with control, *t* test.

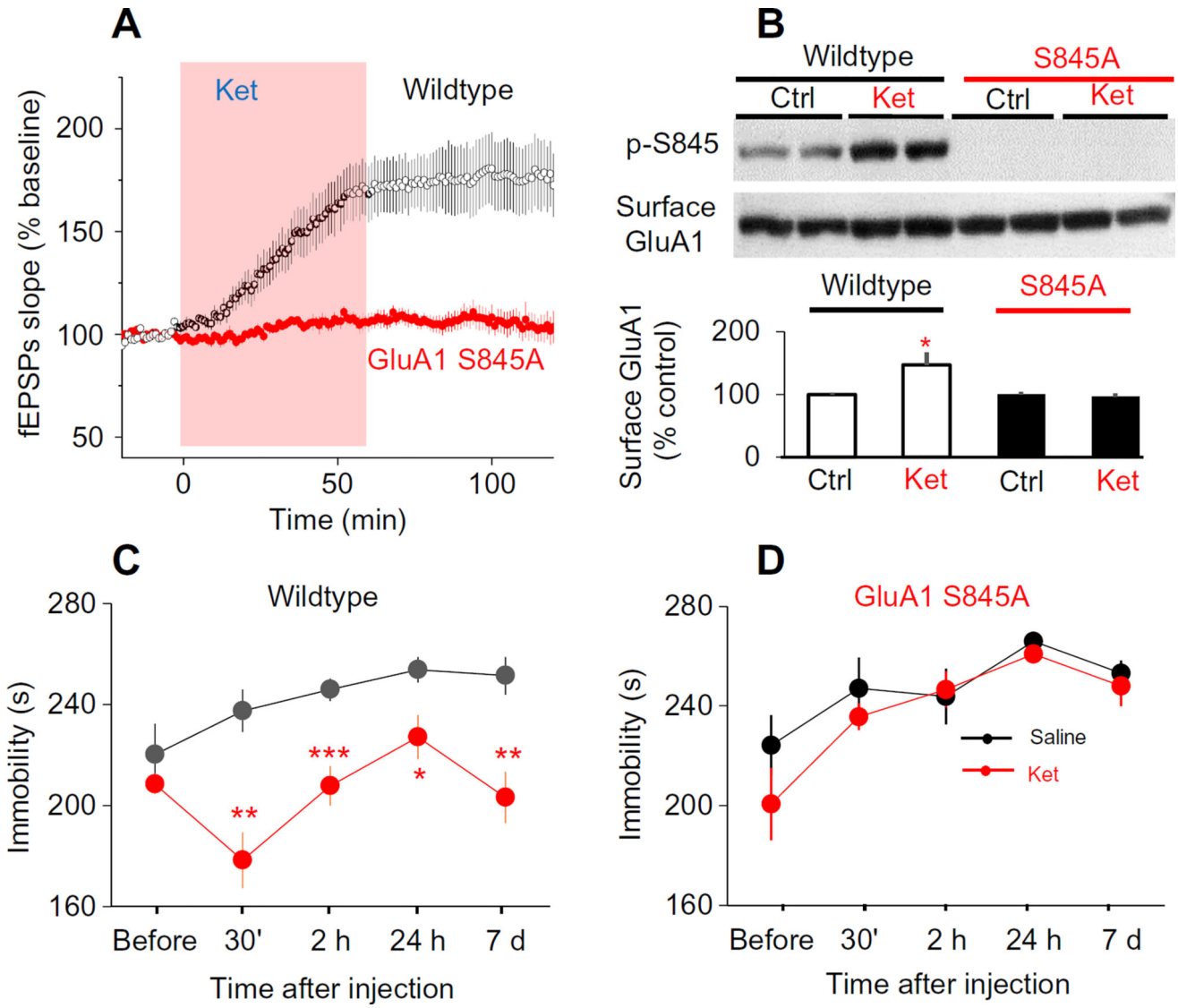

Fig. 4. Phosphorylation of GluA1 Ser^{845} is required for the effect of ket in the FST model of antidepressant action

(**A**) Effect of ket on SC-CA1 fEPSPs in hippocampal slices from wildtype and GluA1 S845A knock-in mice. Acutely prepared mice hippocampal slices were bath-applied with ket (20 μM). Ket enhanced SC-CA1 fEPSPs in wildtype mice but not in GluA1 S845A mutant mice (wildtype: 175 ± 11.4% of baseline, $n = 8$ slices; $P < 0.001$, paired t test; GluA1 S845A mice: 108 ± 4.3% of baseline, $n = 6$ slices; $P = 0.20$, paired t test). (**B**) Effect of ket on the abundance of GluA1 at the cell surface in wildtype and GluA1 S845A knock-in mice. Surface proteins were extracted by biotinylation assay, then GluA1 and Ser^{845} phosphorylated GluA1 (p-S845) were detected by Western blotting. Top: Representative blots. Bottom: Surface GluA1 and GluA1 Ser^{845} phosphorylation quantified from six independent experiments. *$P < 0.05$ compared with control, paired t test. (**C** and **D**) Effect of a single ket injection on animal behavior in the FST for wildtype mice (C) and GluA1 S845A knock-in mice (D). Mice were tested at the indicated times up to 7 days after

injection of ket (10 mg/kg, i.p.) (wildtype mice: $n = 6$; GluA1 S845A mice: $n = 7$. $^{*}P < 0.05$, $^{**}P < 0.01$, and $^{***}P < 0.001$ compared to corresponding time point before ket, paired t test.

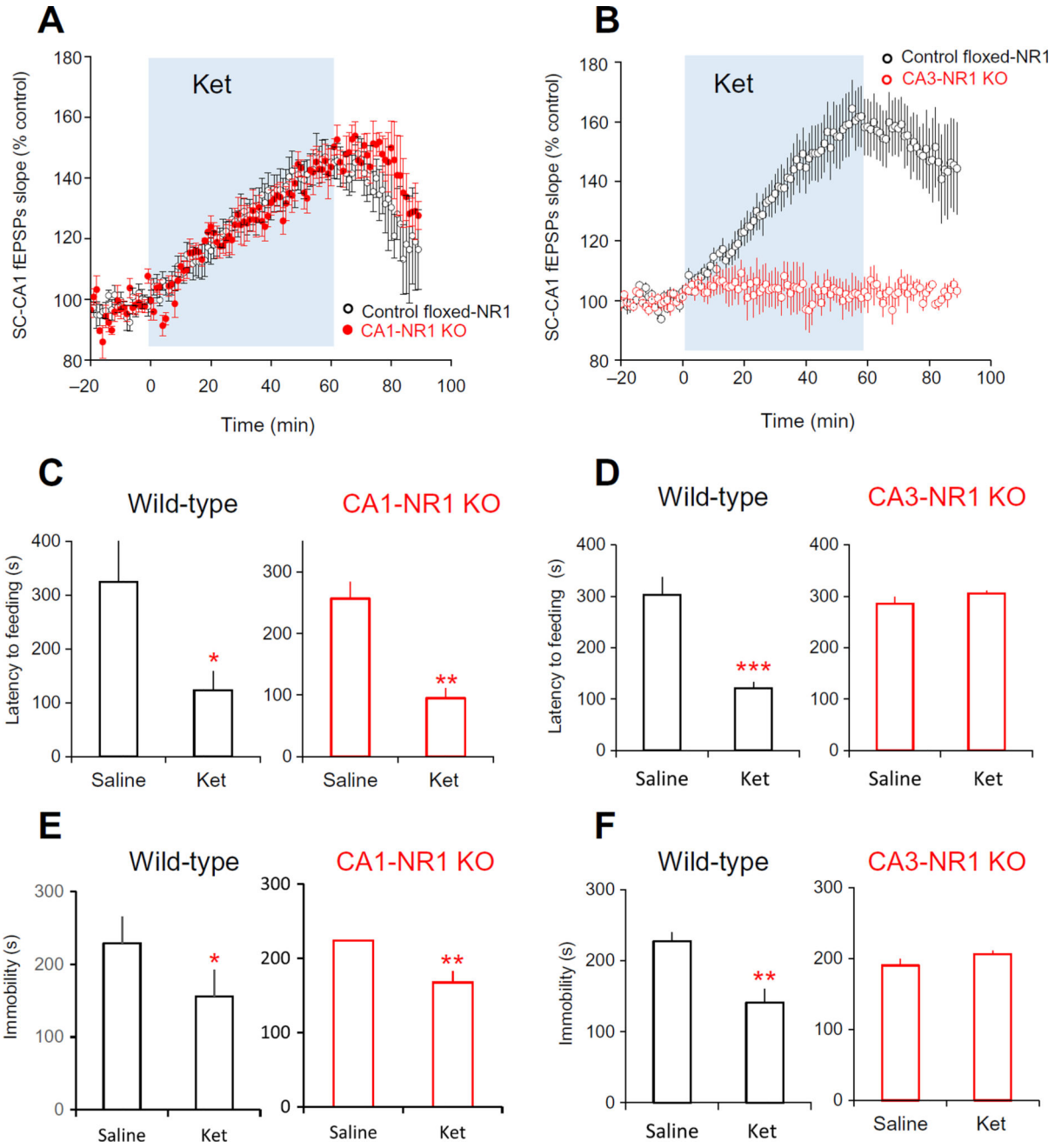

Fig. 5. Presynaptic (CA3) but not the postsynaptic (CA1) NMDARs are required for the antidepressant actions of ket

(**A**) Effect of ket on SC-CA1 fEPSPs in hippocampal slices from control (control floxed-NR1) and CA1-NR1 KO mice. Ket potentiated SC-CA1 fEPSPs in slices from control floxed-NR1 mice and CA1-NR1 KO mice (control floxed-NR1 mice: 139.1 ± 5.1%, $n = 7$ slices from five mice; CA1-NR1 KO mice: 143.3 ± 4.3%, $n = 7$ slices from six mice; $P = 0.42$, t test). (**B**) Effect of ket on SC-CA1 fEPSPs in hippocampal slices from control and CA3-NR1 KO mice. Ket failed to enhance SC-CA1 fEPSPs in slices from CA3-NR1 KO mice (control floxed-NR1 mice: 159.1 ± 12.2%, $n = 8$ slices from four mice; CA3-NR1 KO

mice: 102 ± 4.9%, $n = 7$ slices from four mice; $P = 0.005$, t test). (**C**) Effect of ket on behavior in novelty-suppressed feeding test of control floxed-NR1 mice and CA1-NR1 KO mice. Five mice of each genotype were tested. (**D**) Effect of ket on behavior in novelty-suppressed feeding test of control floxed-NR1 mice and CA3-NR1 KO mice. Five mice of each genotype were tested. (**E**) Effect of ket on behavior in the FST of control floxed-NR1 mice and CA1-NR1 KO mice. Five mice of each genotype were tested. (**F**) Effect of ket on behavior in the FST of control floxed-NR1 mice and CA3-NR1 KO mice. Five mice of each genotype were tested. For (B), (C), (E), and (F), $*P < 0.05$, $**P < 0.01$, and $***P < 0.001$ compared to saline-treated group, unpaired t test.

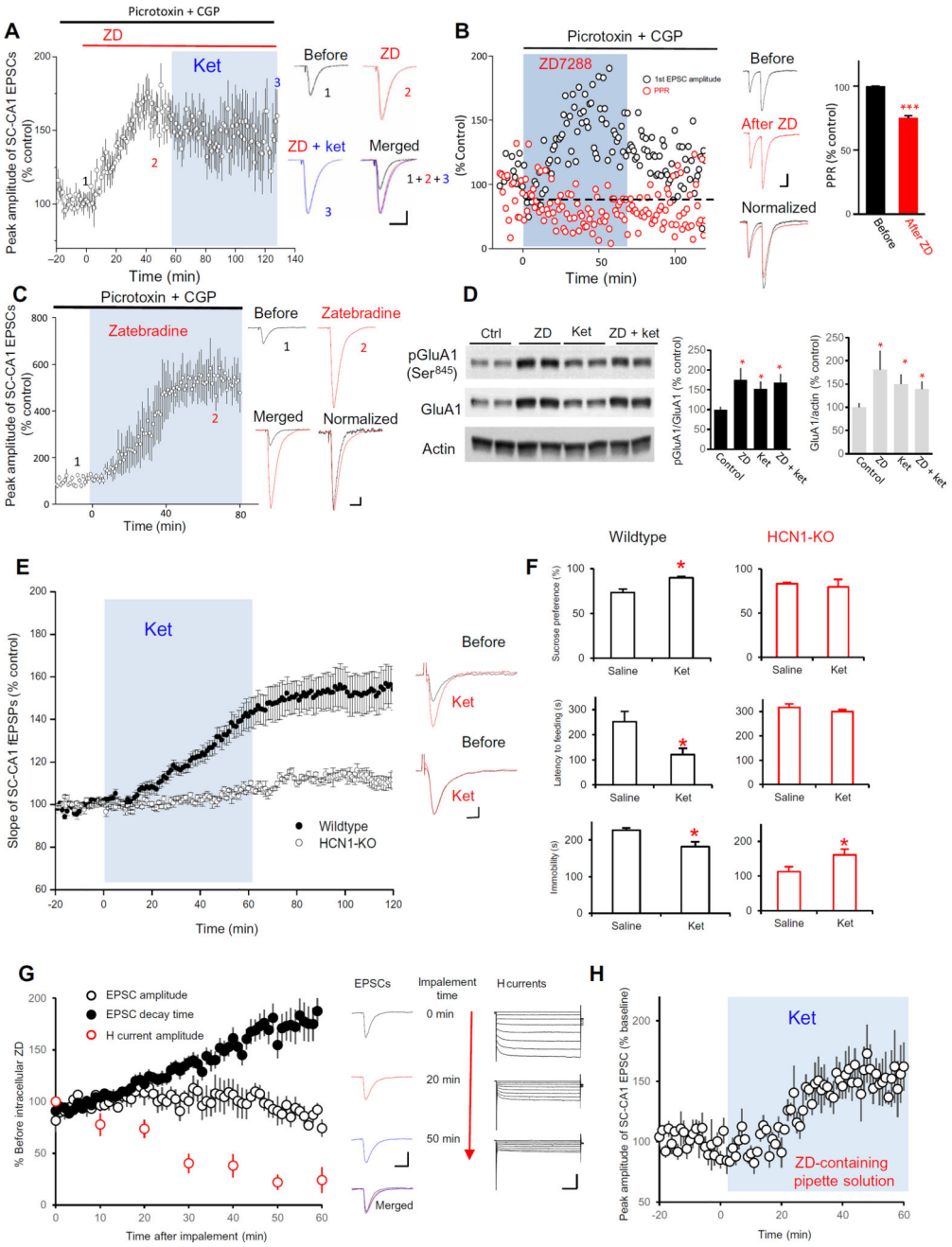

Fig. 6. The synaptic and behavioral actions of ket are mimicked and occluded by HCN channel inhibition or deletion

(**A**) Effect of HCN inhibition by ZD on the peak amplitude of SC-CA1 EPSCs and the ability of ket-induced potentiation. Left: Data were presented as the hippocampal slices were pretreated by picrotoxin (100 μM) and CGP (4 μM) for 30 min and then first bath-applied with ZD (15 μM) followed by combined ket (20 μM) treatment (ZD: 155.6 ± 9.5% of baseline, $n = 7$ cells, $P < 0.05$, paired t test). Right: Representative traces. (1) Baseline treated with picrotoxin and CGP, (2) after ZD application, and (3), after ket plus ZD application; merged traces of 1, 2, and 3. Scale bar, 50 ms/50 pA. SC-CA1 EPSCs were recorded in the presence of picrotoxin and CGP to prevent any effects of GABAergic input.

(**B**) Effect of HCN inhibition by ZD on PPR of SC-CA1 EPSCs. Rat hippocampal slices were recorded in the presence of picrotoxin (100 μM) and CGP (4 μM) to prevent any effects of GABAergic input. Left: Representative data from a single-cell recording are presented as peak amplitude or PPR of SC-CA1 EPSCs normalized to the baseline before ZD (15 μM) application. Middle: Representative traces before and after ZD application as well as merged and normalized (to before ZD) traces. Scale bar, 50 ms/50 pA. Right: Quantified data from seven cells show that ket significantly reduced PPR of SC-CA1 EPSCs (75.3 ± 5.9% of baseline at 50 to 60 min after ZD; ***$P < 0.001$, paired t test). (**C**) Effect of HCN inhibition by zatebradine (10 μM) on SC-CA1 EPSCs. EPSCs were recorded, and data are presented as in (A) (zatebradine: 576.9 ± 87.2% of baseline, $n = 3$ cells; $P < 0.05$, paired t test). Scale bar, 50 ms/50 pA. (**D**) Effect of ZD on GluA1 Ser^{845} phosphorylation (pGluR1) and abundance in the presence and absence of ket. Representative blots (left) and quantified data (right) of five independent Western blot experiment show that ZD occluded ket-induced enhancement of GluA1 phosphorylation and abundance. *$P < 0.05$ compared with control, Tukey's post hoc tests. (**E**) Effect of ket on SC-CA1 fEPSPs in HCN1-KO mice. Ket failed to enhance SC-CA1 fEPSPs in hippocampal slices from HCN1-KO mice (104.1 ± 5.5% of baseline, $n =$ 10 slices from five mice; $P = 0.3611$, paired t test) but significantly enhanced SC-CA1 fEPSPs in slices from wild-type mice (148 ± 8.7% of baseline, $n = 12$ slices from five mice; $P = 0.001$, paired t test). Left: Time course of SC-CA1 fEPSPs slop. Right: Representative traces. Scale bar, 10 ms/0.1 mV. (**F**) Effect of ket in three behavioral tests in wild-type and HCN1-KO mice. Animals were assessed using the sucrose preference test (top), the novelty-suppressed feeding test (middle), and the FST (bottom). *$P < 0.05$; $n = 6$ mice in each saline-treated and ket-treated group. (**G**) Effect of HCN inhibition by ZD dialyzed into CA1 cells on SC-CA1 EPSCs and I_h. ZD (15 μM) was dialyzed through the patch pipette into the CA1 neurons, and SC-CA1 EPSCs were recorded. Amplitude and decay times are shown normalized to the values at the beginning when the cell was impaled by the pipette. Left: Time courses of peak amplitude, decay time of SC-CA1 EPSCs, and peak amplitude of h current during ZD dialysis. Middle: Representative traces of SC-CA1 EPSCs 0, 20, and 50 min after implement. Scale bar, 50 ms/100 pA. Right: Representative h currents measured by comparing the difference between the instantaneous (peak) tail current amplitude and the steady-state current amplitude. Scale bar, 500 ms/300 pA. (**H**) Effect of ket on SC-CA1 EPSCs after HCN inhibition by ZD dialysis into CA1 cells. CA1 neurons were patched with pipette containing with ZD (15 μM) for 1 hour, then ket (20 μM) was applied to the bath solution, and SC-EPSCs were recorded. Ket significantly increased the peak amplitude of SC-CA1 EPSCs (156.1 ± 17.2% of baseline 50 to 60 min after ket, $n = 6$ slices; $P < 0.01$, paired t test).